Two- and Three-Dimensional Self-Folding of Free-Standing Graphene by Liquid Evaporation

Qingchang Liu and Baoxing Xu*

Department of Mechanical and Aerospace Engineering, University of Virginia,

Charlottesville, VA 22904, USA

Abstract: Two-dimensional (2-D) atomically thin graphene has exhibited overwhelming excellent properties over bulk counterpart quantity graphite, yet their broad applications and explorations of unprecedented properties require the diversity of their geometric morphologies, beyond their inherently planar structures. In this study, we present a self-folding approach of converting 2-D planar free-standing graphene to 2-D and 3-D folded structures through the evaporation of its liquid solutions. This approach involves the competition of surface energy of liquid, and deformation energy and van der Waals energy of graphene. An energy-based theoretical model is developed to describe the self-folding process during liquid evaporation by incorporating both graphene dimensions and surface wettability. The critical elastocapillary length by liquid evaporation is extracted and exemplified by investigating three typical graphene geometries with rectangular, circular and triangular shapes. After the complete evaporation of liquid, the critical self-folding length of graphene to a stable folded pattern by van der Waals energy is also obtained. In parallel, full-scale molecular dynamics (MD) simulations are performed to monitor the evolution of deformation energies and folded patterns with liquid evaporation. The simulation results demonstrate the formation of 2-D folded racket-like and 3-D folded cone-like patterns and show remarkable agreement with theoretical predictions in both energy variations and folded patterns. This work offers a quantitative guidance for controlling the self-folding of graphene and other 2-D materials into complex structures by liquid evaporation.

Keywords: graphene; liquid evaporation; surface wettability; self-folding; energy criterion

* Corresponding author: bx4c@virginia.edu

1. Introduction

Graphene and other two-dimensional (2-D) materials have proved to be excellent and unique in numerous properties including mechanical, thermal and electrical properties which rely critically on the atomically thin thickness of structures in nature [1]. In most applications, non-planar structures in geometry are desired to leverage these properties. For example, curved and/or folded architectures of graphene improve the flexibility of the graphene-enabled sensors and actuators [2-4], wrinkled graphene facilitates to achieve mechanically controllable surface wettability[5] and to realize the anisotropic resistance of electrical transport [6], and crumpled graphene is utilized to enhance photo-responsivity of sensors[7] and performance of supercapacitors.[8, 9] These varieties of non-planar geometric structures broaden applications of graphene and also advance the exploration of unprecedented properties in 2-D materials, beyond the inherent planar structures.

A few of strategies have been developed to introduce local or/and global curvatures in 2-D materials, and even to fold them into various patterns so as to achieve on-demand properties. For example, a buckled graphene monolayer and multilayer sheets on a soft substrate are obtained by applying a mechanical loading[10, 11]. For a graphene sheet on a substrate, a folded racket-like pattern could also be formed by van der Waals (vdW) interactions due to instability and has been confirmed in simulations [12, 13]. Recently, the origami concept has been applied to convert graphene into various shapes, and offers great attention for designing deterministic structures of 2-D materials. So far, most folded 2-D materials are achieved by applying a mechanical force[14], or triggered by decorating functional groups [15, 16] or pre-patterning[17].

As an alternative approach, the evaporation-driven folding of 2-D materials is emerging and provides a facile and convenient technique[18]. For example, folding a thin elastic sheet by liquid evaporation, often referred to as elastocapillary phenomenon, is ubiquitous [19-22] and has been utilized to fabricate complex 3-D structures [19, 23]. To fold a free-standing 2-D materials, they are commonly suspended in a liquid solution in advance, and then an elevated temperature will be introduced to dry the mixture. As a consequence, the 2-D sheets could be deformed into different shapes due to elastocapillary. When numbers of 2-D material sheets are mixed with liquid solution, this technique could be used to deform and assemble them into bulk nanostructures meanwhile keeping the large accessible surface area of 2-D materials due to the

resistance of surface curvature to contact at assembly [24-30].

In essence, during the liquid evaporation, the deformation energy of 2-D materials will increase, and the surface energy of liquid will decrease due to the decrease of liquid volume till to complete evaporation. Consequently, their competition determines whether liquid evaporation will promote deformation of 2-D materials and triggers the subsequent self-folding[31-33]. After the complete evaporation of liquid or below a critical amount of volume, where the solid-liquid interaction is very small and can be neglected, the final folded pattern will be determined by the vdW interactive energy (also referred to as binding energy) of 2-D materials. For a graphene nanoribbon or 1-D nanofiber with a large aspect ratio, numerous studies show that deformation and folding are always preferable along the long axis direction because of required small deformation energy[31-34]. However, quantitative study of folding 2-D materials with a comparable dimension in two directions is still lacking, and the effect of surface wettability is also unclear.

In the present study, we will conduct a systematic study of evaporation-driven self-folding of 2-D graphene suspended in a liquid droplet and develop a theoretical model for predicting self-folding process and final folded patterns. The theoretical model is established by considering deformation energy of 2-D solid materials, the surface energy of solid and liquid, interfacial energy between solid and liquid, and vdW (binding) energy of 2-D materials when folded. Geometric features and surface wettability of graphene are also incorporated into the model. Three typical graphene geometries, rectangular and circular shapes which represent an axial symmetry, and triangular shape which represents a central symmetry, are studied. In addition to the self-folded spatial patterns of graphene, the 3-D profile of liquid droplet is also extracted to precisely capture the surface energy of liquid. Theoretical analysis shows that 2-D folded pattern is obtained in the rectangle and circle graphene after complete evaporation of liquid, and the triangle graphene can be folded to a 3-D spatial pattern. The critical elastocapillary and self-folding lengths that determine the self-folding by liquid evaporation and ultimate formation of a stable folded pattern respectively are obtained. Molecular dynamics (MD) simulations are performed to validate the theoretical model and self-folding process of graphene with liquid evaporation. Good agreement between theoretical predictions and simulations is obtained in both folded spatial patterns and sizes.

2. Theoretical model

Consider a single free-standing graphene suspended in a liquid droplet, the total energy of the system is

$$E_{tot} = E_{def} + E_{surf}^{l} + E_{surf}^{g} + E_{inter} + E_{vdW} \quad (1)$$

where $E_{def} = \int_{A_d} \frac{B}{2r_b^2} dA$ is the deformation energy of graphene[23, 34-37], $E_{surf}^{l} = \int_{A_l} \gamma_l dA$ is the surface energy of liquid, $E_{surf}^{g} = \int_{A_g} \gamma_s dA$ is the surface energy of graphene, $E_{inter} = \int_{A_i} \gamma_i dA$ is the interfacial energy between graphene and liquid, and $E_{vdW} = \int_{A_o} \gamma_b dA$ is the binding energy of graphene. A_d is the area of deformed graphene, B is the bending stiffness of graphene, r_b is the radius of curvature, A_l is the surface area of liquid exposed to vacuum/air, γ_l is the surface tension of liquid, A_g is the surface area of graphene exposed to vacuum/air, γ_s is the surface energy density of graphene, A_i is the contact area between solid and liquid, γ_i is the interfacial energy density, A_o is the overlap area in the deformed graphene and γ_b is the vdW binding energy density of overlap area. Once the liquid evaporation begins, the surface energy of liquid will decrease, i.e. $\Delta E_{surf}^{l} < 0$, and the capillary force will deform the graphene sheet to achieve a conformal contact between them. As a consequence, the deformation energy of graphene will increase, i.e. $\Delta E_{def} > 0$, leading to a competition between surface energy of liquid and deformation energy of graphene. Depending on the contact status between liquid and graphene, both interfacial energy and binding energy of graphene may also change, and when the total energy of system keeps decreasing, i.e. $\Delta E_{tot} < 0$, and $\Delta E_{def} > 0$, the liquid evaporation-induced deformation of graphene will continue, and otherwise, $\Delta E_{tot} > 0$ or $\Delta E_{tot} < 0$ and $\Delta E_{def} < 0$, the folding will stop and no further folding will occur.

2.1 Elastocapillary by liquid evaporation

At the beginning of evaporation, there is no overlap in graphene and A_o=0, and thus $E_{vdW} = 0$. The graphene will stay in contact with the outmost surface of water droplet with one surface side exposed to the vacuum/air due to the requirement of the minimum system energy, and $A_d = A_g = A_i$. Take the rectangular graphene with length l and width w $(l \geq w)$ as an

example, as illustrated in Fig. 1a, and assume the deformation is unidirectional along its long symmetric axis, r_b is a constant across the entire deformed graphene with the bending angle θ_b, and $\theta_b = l/2r_b$, Eq. (1) is simplified to

$$E_{tot} = \frac{2B\theta_b^2}{\eta} + A_l\gamma_l + lw\gamma_s + lw\gamma_i \quad (2)$$

where $\gamma_i = \gamma_s - \gamma_l cos\theta_c$ [38], θ_c is the contact angle and $\eta = l/w$. The surface area of liquid A_l will vary with θ_b (S1 in supplemental materials for details). With these geometric relationships, for rectangular shape, the energy analysis shows that the self-folding deformation along the long symmetric axis is preferable in energy in comparison with along the short axis, consistent with that of graphene nanoribbons [39], as shown in Fig. S8.

After the folding direction is determined, with liquid evaporation, the bending angle of graphene θ_b will increase. As discussed above, both surface energy of graphene $lw\gamma_s$ and interfacial energy $lw\gamma_i$ remain constant, the total energy E_{tot} in Eq. (2) is a function of θ_b via the first and second terms and can be solved through numerical iterations, as shown in supplemental materials S1. Therefore, a successful self-folding by liquid evaporation requires $E_{tot}(\theta_b + \Delta\theta_b) < E_{tot}(\theta_b), (\Delta\theta_b > 0, \theta_b \in [0, \pi])$. Define $\Delta E_{tot}(\theta_b) = E_{tot}(\theta_b + \Delta\theta_b) - E_{tot}(\theta_b)$, if $\Delta E_{tot}(\theta_b) < 0$, the evaporation-induced folding can be achieved and a fully wrapped state of graphene with liquid droplet will be obtained. As a consequence, from Eq. (2), we will have

$$\Delta E_{tot} = \Delta E_{def} + \Delta E_{surf}^{l} \quad (3)$$

where $\Delta E_{def} = \frac{2B}{\eta}[(\theta_b + \Delta\theta_b)^2 - \theta_b^2]$ represents the increase of deformation energy of graphene and $\Delta E_{surf}^{l} = A_l(\theta_b + \Delta\theta_b)\gamma_l - A_l(\theta_b)\gamma_l$ represents the decrease of surface energy of liquid. Therefore, the criterion for a successful folding process by liquid evaporation can be defined as

$$\left|\frac{\Delta E_{def}}{\Delta E_{surf}^{l}}\right| < 1, (\theta_b \in [0, \pi]) \quad (4)$$

The critical self-folding length of graphene can be calculated via $\left|\Delta E_{def}/\Delta E_{surf}^{l}\right|_{\theta_b=\pi} = 1$ and it is $l_{ec} = \sqrt{4\pi^3/(\eta + \pi)}\sqrt{B/\gamma_l}$ (S2 in supplemental materials for details).

Following the similar analysis, we also determine the profile and energy for the liquid

evaporation-driven folding of circular and triangular graphene (Fig.1b and Fig. 1c, S1 in supplemental materials). For circular graphene, the folding line could be arbitrary diameter (Fig. 1b), and the analysis leads to l_{ec} =6.32$\sqrt{B/\gamma_l}$. For triangular graphene, unlike the axisymmetric folding of rectangular and circular graphene, its self-folding will be conducted along centrosymmetric direction (Fig.1c), and we can have $l_{ec} = 3.45\sqrt{B/\gamma_l}$. By introducing a geometric factor, s, the critical length of these three graphene geometries can be unified into (S2 in supplemental materials for details)

$$l_{ec} = s\sqrt{\frac{B}{\gamma_l}} \tag{5}$$

where $\sqrt{B/\gamma_l}$ represents the material constants of solid and liquid, and $s = \sqrt{4\pi^3/(\eta + \pi)}$ (Rectangle), 6.32 (Circle) and 3.45 (Triangle). In particualr, for retangular graphene with a small aspect ratio, i.e. $\eta \ll 1$, $s = 2\pi$, and the citical length l_{ec} in Eq. (5) will be the same with that of graphene nanoribbons [32].

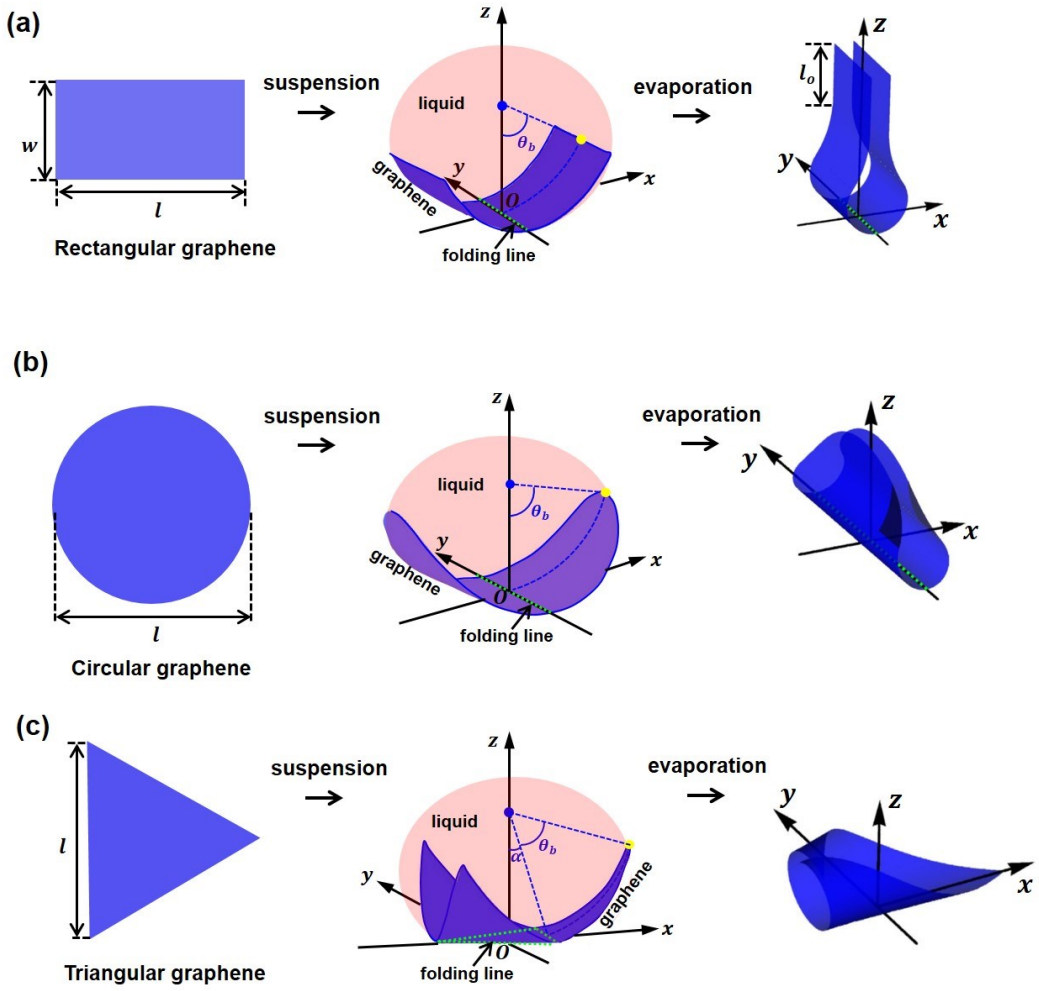

Figure 1. Evaporation-driven self-folding of a single suspended graphene sheet in a liquid environment. Schematics of planar **(a)** rectangular, **(b)** circular and **(c)** triangular graphene, their suspended in liquid and self-folded pattern after complete evaporation of liquid. l and/or w are size of planar graphene. θ_b is the bending angle of graphene in liquid. l_o is the length of overlap part.

2.2 Effect of surface wettability

In the determination of l_{ec} in Eq. (5), a full contact between graphene and liquid droplet is assumed, associated with a constant interfacial energy during evaporation. Essentially, l_{ec} in Eq. (5) reflects the energy competition between liquid surface and deformation of graphene. However, the detaching between graphene and liquid may happen during the folding of graphene with liquid evaporation, as illustrated in Fig. 2. In particular, when the effect of surface wettability of graphene is considered[40, 41], the interfacial energy may change with evaporation. Besides, once the graphene does not remain in contact with liquid surface, the

detached section will recover to be planar [42, 43]. Consider the surface area of detached graphene A_s (>0), the total energy of the system in Eq. (2) will become

$$E_{tot} = \frac{B(lw-A_s)}{2r_b^2} + (A_l + A_s)\gamma_l + (lw + A_s)\gamma_s + (lw - A_s)\gamma_i \quad (6)$$

The energy difference between the scenarios with full (Eq. (2), E_{tot}^{fold}) and partial contact (Eq. (6), E_{tot}^{detach}) between graphene and water is $\Delta E_{tot}^{d-f} = E_{tot}^{detach} - E_{tot}^{fold}$, and define the surface wettability of graphene θ_c, we can have (S3 in supplemental materials for details)

$$\Delta E_{tot}^{d-f} = A_s\left[-\frac{B\theta_b^2}{2l^2} + \gamma_l(1 + cos\theta_c)\right] \quad (7)$$

at $\Delta E_{tot}^{d-f} > 0$, no detaching occurs, and the folding will continue with a full contact between liquid and graphene, and otherwise, detachment will happen and self-folding will stop. Apparently, a hydrophobic surface (larger θ_c) will promote the detachment and suppresses the self-folding process. With the consideration of this effect of surface wettability, the critical length of graphene that can be folded by evaporation, here referred to as wet-capillary critical length l_{wc}, can be derived via $\Delta E_{tot}^{d-f} = 0$ and it is (S3 in supplemental materials for details)

$$l_{wc} = g\sqrt{\frac{B}{2\gamma_l(1+cos\theta_c)}} \quad (8)$$

where g is the geometry factor and $g = \pi$ for rectangular and circular graphene, and $g = 2.9\pi/\sqrt{3}$ for triangular graphene.

The comparison between Eqs. (5) and (8) shows that the critical length of graphene to be folded by liquid evaporation will be determined by both the size dimension and surface wettability of graphene, rather than by the sole size dimension via l_{ec}. For example, given the aspect ratio η, bending stiffness B of a rectangular graphene and surface tension γ_l of liquid, a critical contact angle θ_c^c can be derived by $l_{ec} = l_{wc}$, which yields $\theta_c^c = acos(\eta/8\pi - 7/8)$. When $\theta_c < \theta_c^c$, $l_{ec} > l_{wc}$ and a successful folding process requires $l > l_{ec}$, and when $\theta_c \geq \theta_c^c$, a successful folding process requires $l > l_{wc}$.

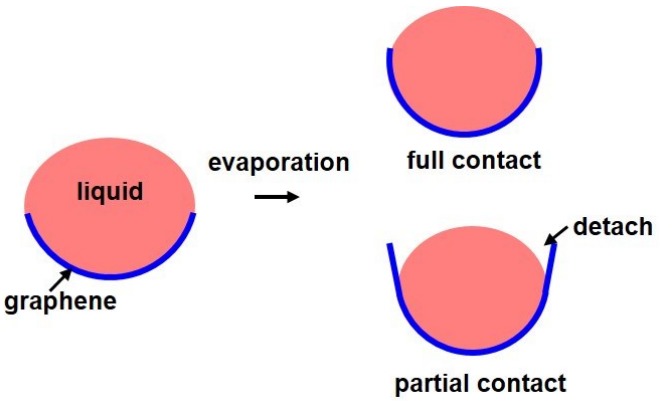

Figure 2. Schematic illustrations (side view) of full and partial contact of graphene with liquid droplet.

2.3 Van der Waals (vdW) energy-driven self-folding

With the continuous evaporation of liquid and self-folding of graphene, the deformed graphene starts to contact with each other ($A_o > 0$), where the vdW binding energy E_{vdW} needs to be considered [32]. Take the rectangular graphene as an example, the total energy of the system now becomes

$$E_{tot} = \frac{B(l-2l_o)w}{2r_b^2} + A_l\gamma_l + lw\gamma_s + (lw - 2l_ow)\gamma_i + l_ow\gamma_b \quad (9)$$

where l_o is the overlap length ($A_o = l_ow$, as illustrated in Fig. 1a) and γ_b is the binding energy density of graphene ($=-0.232J/m^2$ [12]). In this stage, because most water has been evaporated, the surface energy of liquid can be neglected and the interfacial energy between solid and liquid could be replaced by the surface energy of solid in theoretical analysis. After the complete evaporation of liquid, the folded solid will be independent of liquid and the variation of total energy is

$$\Delta E_{tot} = \Delta E_{def} + \Delta E_{surf}^{g} + \Delta E_{vdW} \quad (11)$$

With the liquid evaporation, a continuous folding of graphene will lead to $\Delta E_{tot} < 0$, $\Delta E_{def} > 0$, $\Delta E_{surf}^{g} < 0$ and $\Delta E_{vdW} < 0$, and therefore the successful self-folding process of graphene will require

$$\left|\frac{\Delta E_{def}}{\Delta E_{surf}^{g} + \Delta E_{vdW}}\right| < 1 \quad (12)$$

During the self-folding process, $\left|\Delta E_{def}/(\Delta E_{surf}^{g} + \Delta E_{vdW})\right|$ will increase until to equaling

to 1 where a stable self-folded arrives, and the overlap length in the folded graphene l_o can be obtained via $\left|\Delta E_{def}/(\Delta E_{surf}^{g}+\Delta E_{vdW})\right|$=1. Accordingly, the critical self-folding length l_{cr} due to vdW energy can be determined by $\left|\Delta E_{def}/(\Delta E_{surf}^{g}+\Delta E_{vdW})\right|_{l_o=0}=1$ and it is (S4 in supplemental materials)

$$l_{cr}=k\sqrt{\frac{B}{|\gamma_b-2\gamma_s|}} \tag{13}$$

where $k=2\pi$ for rectangle, k=11.72 for circle and k=13.57 for triangle.

3. Computational modeling and simulations

To validate the theoretical analysis, full-scale molecular dynamics (MD) simulations were conducted using LAMMPS[44]. SPC/E model was used to model water molecules[45], and the AIREBO force field was employed to model graphene[46, 47]. The 12-6 Lennard-Jones (L-J) non-bonded pairwise potential $V_{L-J}(r)=4\varepsilon_{c-o}(\sigma^{12}/r^{12}-\sigma^{6}/r^{6})$ was used to model the carbon-water vdW interactions, where ε_{c-o} is the potential well depth, σ is the equilibrium distance and r is the distance between two atoms. The coulomb interaction $V_q(r)=q_iq_j/4\pi\varepsilon_0 r$ was used to model the electrostatic interaction between water molecules i and j. The cut-off radius of 1.0 nm was chosen, and the particle-particle-particle-mesh (PPPM) with a root mean of 0.0001 was employed to calculate the long-range Coulomb interactions between oxygen and hydrogen atoms in water molecules. Periodic boundary conditions were applied in the x, y and z directions of the simulation cubic box that was far larger than the graphene-water system to avoid the effect of periodic image[37, 48].

The simulations of liquid evaporation included three major steps. First, the equilibrium of system consisting of 21296 water molecules and a graphene sheet was reached under the NVT ensemble with Nose/Hoover thermostat at 300K at 1.0 atmosphere. The simulations were run for 1.0 ns with time step of 1.0 fs. Second, water molecules were removed randomly to mimic evaporation of liquid and the evaporation rate was 10000 water molecules per nanosecond under the NVE ensemble. Afterward, the system would be re-equilibrated under NVE ensemble to ensure a slow liquid evaporation without affecting the deformation of graphene. The evaporation and equilibrium procedures were repeated until all the water molecules were removed completely. During these process, the coordinates of atoms in both water and

graphene were monitored every 10000 time steps to ensure to document enough data. Third, the NVE ensemble was run for another 1.0 ns after the complete evaporation of water molecules to make sure the arrival of a folded stable graphene.

4. Results

Fig. 3a illustrates the comparison of the volume of water (V_l) and deformation of graphene (θ_b) between the theoretical and simulation results for rectangular planar graphene. With the decrease of volume of water (evaporation), the bending angle of graphene increase (folding), and good agreement between simulations and theoretical analysis is observed. Moreover, Fig.3b shows that both profiles of water and graphene during simulation are well consistent with theoretical predictions. Fig.3c shows the history of surface energy of liquid E_{surf}^{l}, deformation energy of graphene E_{def} and binding energy of the overlap part in the graphene E_{vdW} with evaporation. During the equilibrium process, E_{surf}^{l} shows an obvious decrease due to the minimization of liquid surface energy, and E_{def} and E_{vdW} do not change due to the large volume of water. Upon liquid evaporation begins, at the elastocapillary folding stage, E_{surf}^{l} continues to decrease, E_{def} increases steadily and E_{vdW} remains to be an approximate zero, indicting the deformation of graphene yet without any overlap, which validates the assumption made in the derivations of Eqs. (3) and (5) in Section 2.1. As the evaporation continues, an overlap appears in the closest region of folded graphene, and E_{vdW} starts to dominate the folding, as discussed in Section 2.3, showing a decrease till to a constant that corresponds to the formation of a folded stable pattern. At the same time, E_{def} increases rapidly and reaches a constant along with E_{vdW}, and E_{surf}^{l} quickly decreases to zero due to the evaporation of water molecules. Fig. 3d and e shows the energy ratio of these two stages, $\left|\Delta E_{def}/\Delta E_{surf}^{l}\right|$ and $\left|\Delta E_{def}/(\Delta E_{surf}^{g}+\Delta E_{vdW})\right|$, respectively, and the representative snapshots of graphene deformation and water droplet profile (insets in Fig. 3d). A closed pattern is obtained at the end of the elastocapillary folding by liquid evaporation, and an ultimately stably racket-like pattern is formed at the end of the self-folding by vdW energy. Given the bending stiffness of graphene B for a specific length l and width w, and surface tension of

water γ_l, the theoretical energy ratios can be calculated based on Eqs. (4) and (12) and are also plotted in Figs. 3d and e. Good agreement in both stages is observed between simulations and theoretical analysis.

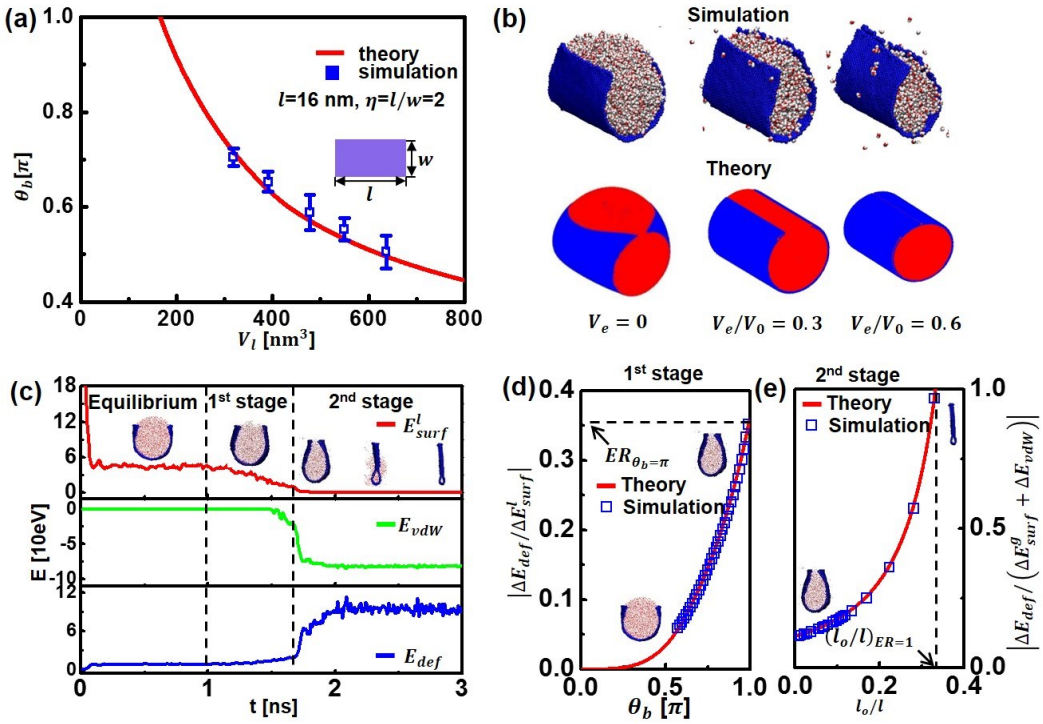

Figure 3. Self-folding deformation and energy variation of graphene with initial planar rectangular geometry with liquid evaporation. (a) Variation of bending deformation-bending angle θ_b of graphene with volume of water V_l. **(b)** Comparison of deformation configuration of graphene and water droplet with evaporation between simulations and theoretical analysis (V_0 is the initial volume of water and V_e is the evaporated volume of water). **(c)** Variation of liquid surface energy E^l_{surf}, binding energy in overlap parts of graphene E_{vdW} and deformation energy of graphene E_{def} with simulation time. Insets show the MD snapshots of graphene deformation in liquid. **(d)** Comparison of the energy ratio $\left|\Delta E_{def}/\Delta E^l_{surf}\right|$ and $\left|\Delta E_{def}/(\Delta E_{vdW}+\Delta E^g_{surf})\right|$ in the elastocapillary mechanism driven by liquid evaporation (1st stage) and self-folding mechanism driven by vdW energy (2nd stage) between simulations and theoretical analysis. The size dimension of rectangular graphene: l=16 nm and η=2, and surface wettability: $\theta_c = 60^\circ$.

Figs. 4 and 5 give the comparison between theoretical analysis and simulations for graphene with circular and triangular shapes, respectively, including deformation of graphene, profile of water droplet and variations of energy. Similarly, good agreement is also obtained. we should mentioned that for the triangular graphene, due to its centrosymmetric folding type, the maximum bending angle is different from that of axisymmetric folding cases (rectangle and circle) and this maximum bending angle can be determined based on the geometric characteristic of triangle (θ_b^{max}=0.72π, S1 in supplemental materials).

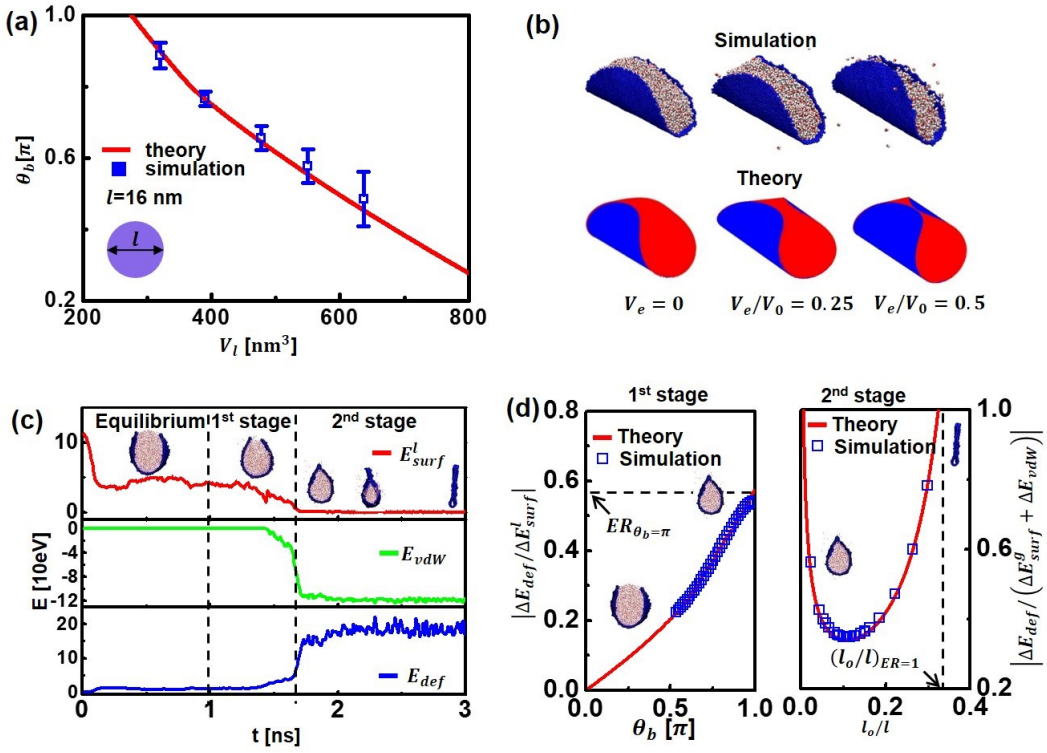

Figure 4. Self-folding deformation and energy variation of graphene with initial planar circular geometry with liquid evaporation. (a) Variation of bending deformation-bending angle θ_b of graphene with volume of water V_l. **(b)** Comparison of deformation configuration of graphene and water droplet with evaporation between simulations and theoretical analysis (V_0 is the initial volume of water and V_e is the evaporated volume of water). **(c)** Variation of liquid surface energy E^l_{surf}, binding energy in overlap parts of graphene E_{vdW} and deformation energy of graphene E_{def} with simulation time. Insets show the MD snapshots of graphene deformation in liquid. **(d)** Comparison of the energy ratio $\left|\Delta E_{def}/\Delta E^l_{surf}\right|$ and $\left|\Delta E_{def}/(\Delta E_{vdW}+\Delta E^g_{surf})\right|$ in the elastocapillary mechanism driven by liquid evaporation (1st stage) and self-folding mechanism driven by vdW energy (2nd stage) between simulations and theoretical analysis. The size dimension of circular graphene: l=16 nm, and surface wettability: $\theta_c = 60^\circ$.

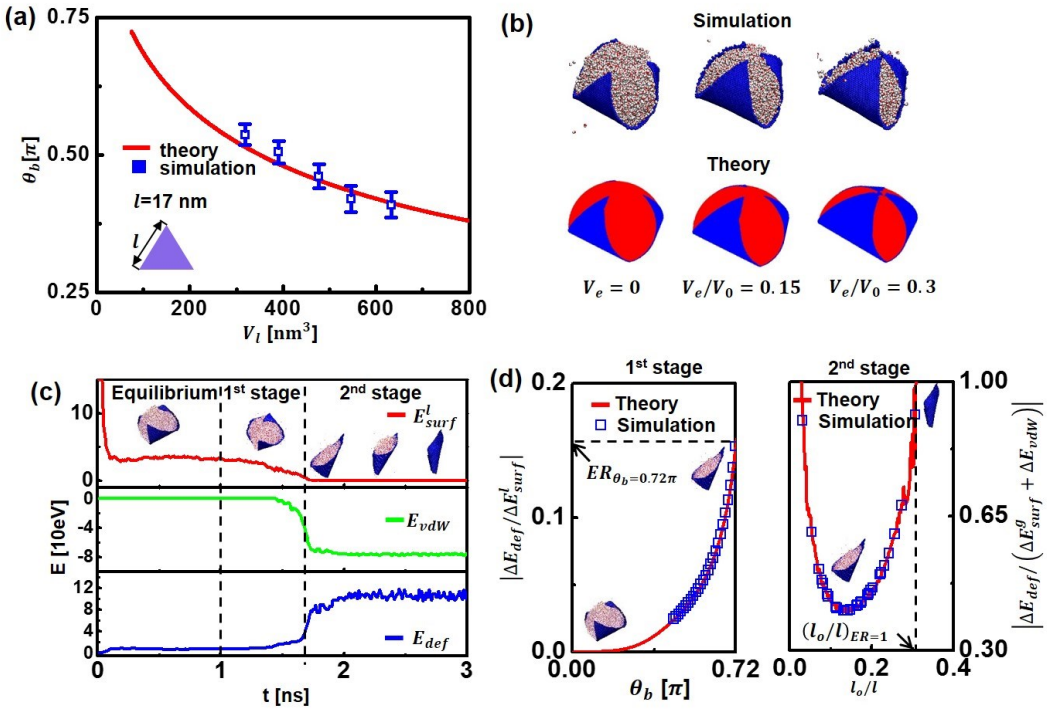

Figure 5. Self-folding deformation and energy variation of graphene with initial planar triangular geometry with liquid evaporation. (a) Variation of bending deformation-bending angle θ_b of graphene with volume of water V_l. **(b)** Comparison of deformation configuration of graphene and water droplet with evaporation between simulations and theoretical analysis (V_0 is the initial volume of water and V_e is the evaporated volume of water). **(c)** Variation of liquid surface energy E^l_{surf}, binding energy in overlap parts of graphene E_{vdW} and deformation energy of graphene E_{def} with simulation time. Insets show the MD snapshots of graphene deformation in liquid. **(d)** Comparison of the energy ratio $\left|\Delta E_{def}/\Delta E^l_{surf}\right|$ and $\left|\Delta E_{def}/(\Delta E_{vdW} + \Delta E^g_{surf})\right|$ in the elastocapillary mechanism driven by liquid evaporation (1st stage) and self-folding mechanism driven by vdW energy (2nd stage) between simulations and theoretical analysis. The size dimension of triangular graphene: l=17 nm, and surface wettability: $\theta_c = 60^\circ$.

With the continuous evaporation of liquid, once there is an overlap in the folded graphene, the theoretical analysis shows that the binding energy starts to dominate the subsequent folding process. In the MD simulations, the rectangular and circular graphene will be folded into a 2-D "racket-like" pattern. In contrast, for the triangular graphene, it will be folded into a 3-D "cone-like" structure. Fig. 6 gives the comparison of the overall configuration of the final patterns folded from planar rectangular, circular and triangular graphene, and all agree with theoretical analyses. Further, Fig. 7a and b plots the overlap length normalized by original size, l_o/l for the folded 2-D racket-like pattern, and good agreement between theoretical analysis and simulations for both folded patterns is obtained. To characterize the 3-D folded cone-like

pattern, two parameters, the ending radius r_e at the "mouth" and the initial radius r_i at the "bottom" are extracted to describe this structure and are given in Fig. 7c. Remarkable agreement between simulations and theoretical analysis is also observed.

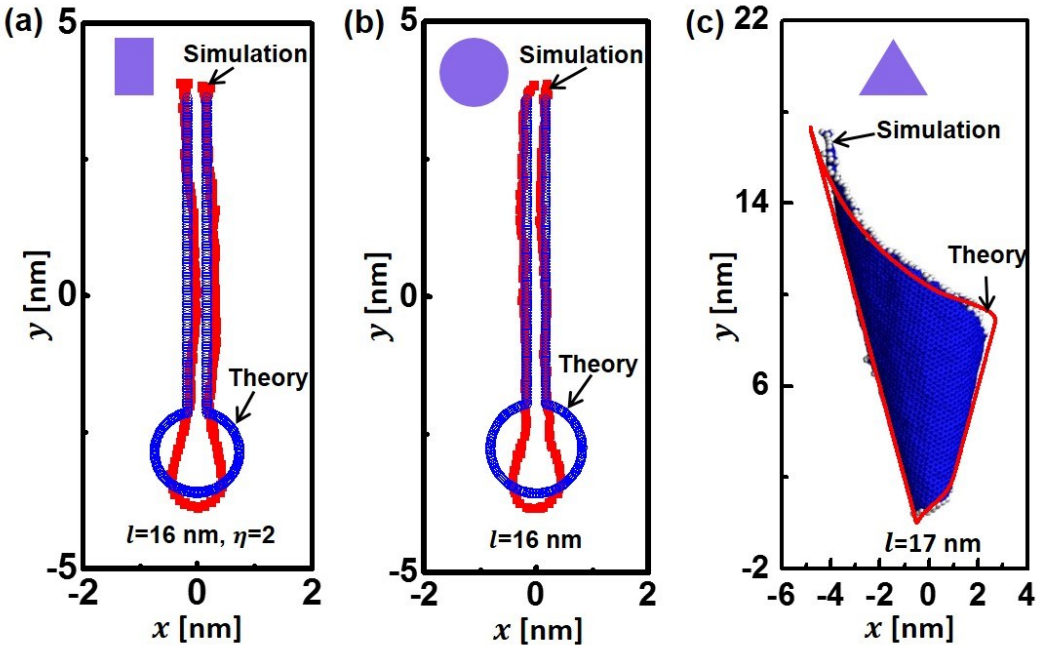

Figure 6. Comparison of overall configurations of self-folded graphene after complete evaporation of liquid between simulations and theoretical analysis. "Racket-like" pattern folded from planar **(a)** rectangular graphene with a length of l=16 nm, and **(b)** circular graphene with a length of l=16 nm. **(c)** "Cone-like" pattern folded from planar triangular graphene with a length of l=17 nm. Surface wettability of graphene in water $\theta_c = 60^\circ$.

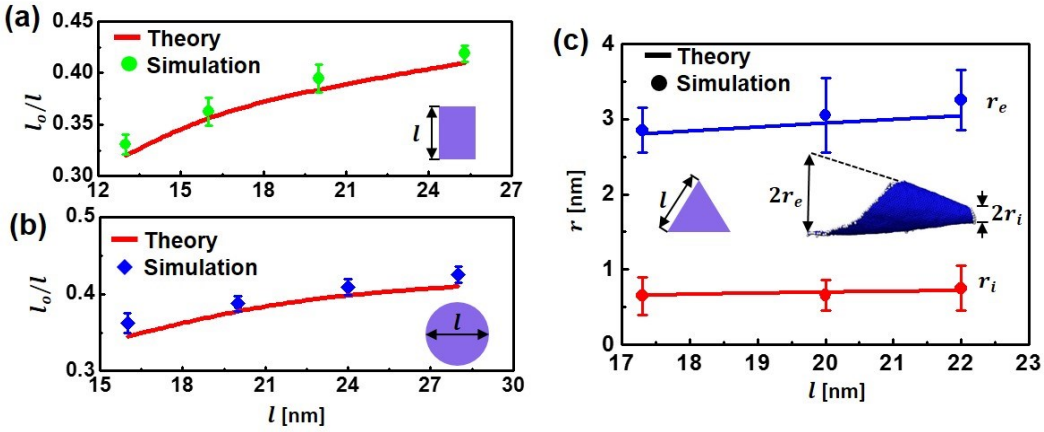

Figure 7. Parametric characterizations of self-folded profile of graphene after complete evaporation of water. 2-D "Racket-like" pattern folded from **(a)** rectangular and **(b)** circular graphene. **(c)** 3-D "Cone-like" pattern folded from triangular graphene. Surface wettability of graphene in water $\theta_c = 60^\circ$.

5. Conclusion

We propose a theoretical framework to describe the self-folding process of graphene by liquid evaporation. The unified theoretical model is built by considering the energy competition of solid deformation, liquid surface and solid-liquid interface, and the effect of surface wettability is also incorporated. Three representative geometries of graphene sheet, rectangular, circular and triangular shapes, are studied. The theoretical analysis shows that the ultimate success of self-folding of graphene is determined by both liquid evaporation-induced and vdW energy-induced self-folding processes, where the former will trigger the self-folding, and the latter will determine stability of self-folded pattern. In particular, in the determination of the critical self-folding length of graphene by liquid evaporation, our theory indicates that a sole elastocapillary length of graphene is not sufficient and the effect of surface wettability needs to be taken into account. A new critical length, referred to as wet-capillary length, is given by considering the variation of interfacial energy during liquid evaporation, and the liquid-evaporation-triggered self-folding of graphene relies on the competition with elastocapillary length and wet-capillary length. Further, the critical length of graphene induced by vdW energy is determined by analyzing competition between deformation energy and binding energy. For different shapes of graphene (axial or central symmetry), the modes of deformation change, and eventually leads to various folded configurations, including 2-D “racket-like” for graphene with axial symmetry in geometry, and 3-D “cone-like” for graphene with central symmetry in geometry. The parallel full-atom molecular dynamics (MD) simulations are conducted to verify theoretical models from energy evolution and liquid droplet profile with liquid evaporation, to the final folded patterns and sizes, and show good agreement with theoretical analysis. The proposed framework could be easily extended to study self-folding of other 2-D materials by updating the geometric parameters in the models and provides a quantitative guidance on the conversion of 2-D materials into other non-planar structures by liquid evaporation required by broad applications of 2-D materials.

Acknowledgement

This work is supported by University of Virginia and NSF-CMMI-1728149.

References

1. D. Akinwande, C. J. Brennan, J. S. Bunch, P. Egberts, J. R. Felts, H. Gao, R. Huang, J.-S. Kim, T. Li and Y. Li, *Extreme Mechanics Letters*, 2017.
2. M. G. Chung, D.-H. Kim, D. K. Seo, T. Kim, H. U. Im, H. M. Lee, J.-B. Yoo, S.-H. Hong, T. J. Kang and Y. H. Kim, *Sensors and Actuators B: Chemical*, 2012, **169**, 387-392.
3. C. Yan, J. Wang, W. Kang, M. Cui, X. Wang, C. Y. Foo, K. J. Chee and P. S. Lee, *Advanced materials*, 2014, **26**, 2022-2027.
4. Y. Wang, R. Yang, Z. Shi, L. Zhang, D. Shi, E. Wang and G. Zhang, *ACS nano*, 2011, **5**, 3645-3650.
5. J. Zang, S. Ryu, N. Pugno, Q. Wang, Q. Tu, M. J. Buehler and X. Zhao, *Nature materials*, 2013, **12**, 321-325.
6. W. Zhu, T. Low, V. Perebeinos, A. A. Bol, Y. Zhu, H. Yan, J. Tersoff and P. Avouris, *Nano letters*, 2012, **12**, 3431-3436.
7. P. Kang, M. C. Wang, P. M. Knapp and S. Nam, *Advanced Materials*, 2016, **28**, 4565-4565.
8. S. Zhang and N. Pan, *Journal of Materials Chemistry A*, 2013, **1**, 7957-7962.
9. Y. Zhou, X.-C. Hu, Q. Fan and H.-R. Wen, *Journal of Materials Chemistry A*, 2016, **4**, 4587-4591.
10. T. Jiang, R. Huang and Y. Zhu, *Advanced Functional Materials*, 2014, **24**, 396-402.
11. K. Zhang and M. Arroyo, *Journal of the Mechanics and Physics of Solids*, 2014, **72**, 61-74.
12. X. Meng, M. Li, Z. Kang, X. Zhang and J. Xiao, *Journal of Physics D: Applied Physics*, 2013, **46**, 055308.
13. S. Cranford, D. Sen and M. J. Buehler, *Applied Physics Letters*, 2009, **95**, 123121.
14. X. Chen, L. Zhang, Y. Zhao, X. Wang and C. Ke, *Journal of Applied Physics*, 2014, **116**, 164301.
15. K. Kim, Z. Lee, B. D. Malone, K. T. Chan, B. Alemán, W. Regan, W. Gannett, M. F. Crommie, M. L. Cohen and A. Zettl, *Physical Review B*, 2011, **83**.
16. R. L. Whitby, V. M. Gun'ko, A. Korobeinyk, R. Busquets, A. B. Cundy, K. László, J. Skubiszewska-Zięba, R. Leboda, E. Tombácz and I. Y. Toth, *ACS nano*, 2012, **6**, 3967-3973.
17. B. Wang, M. Huang, N. Y. Kim, B. V. Cunning, Y. Huang, D. Qu, X. Chen, S. Jin, M. Biswal, X. Zhang, S. H. Lee, H. Lim, W. J. Yoo, Z. Lee and R. S. Ruoff, *Nano letters*, 2017, **17**, 1467-1473.
18. B. Xu and J. A. Rogers, *Extreme Mechanics Letters*, 2016, **7**, 44-48.
19. C. Py, P. Reverdy, L. Doppler, J. Bico, B. Roman and C. N. Baroud, *Physical review letters*, 2007, **98**, 156103.
20. A. Antkowiak, B. Audoly, C. Josserand, S. Neukirch and M. Rivetti, *Proceedings of the National Academy of Sciences*, 2011, **108**, 10400-10404.
21. N. D. Brubaker and J. Lega, *Philosophical transactions. Series A, Mathematical, physical, and engineering sciences*, 2016, **374**.
22. R. W. Style, A. Jagota, C.-Y. Hui and E. R. Dufresne, *Annual Review of Condensed Matter Physics*, 2017, **8**, 99-118.

23. B. Roman and J. Bico, *Journal of physics. Condensed matter : an Institute of Physics journal*, 2010, **22**, 493101.
24. J. Luo, H. D. Jang, T. Sun, L. Xiao, Z. He, A. P. Katsoulidis, M. G. Kanatzidis, J. M. Gibson and J. Huang, *ACS nano*, 2011, **5**, 8943-8949.
25. Y. Chen, F. Guo, A. Jachak, S. P. Kim, D. Datta, J. Liu, I. Kulaots, C. Vaslet, H. D. Jang, J. Huang, A. Kane, V. B. Shenoy and R. H. Hurt, *Nano letters*, 2012, **12**, 1996-2002.
26. X. Ma, M. R. Zachariah and C. D. Zangmeister, *Nano letters*, 2012, **12**, 486-489.
27. K. Sohn, Y. Joo Na, H. Chang, K. M. Roh, H. Dong Jang and J. Huang, *Chemical communications*, 2012, **48**, 5968-5970.
28. W. N. Wang, Y. Jiang and P. Biswas, *The journal of physical chemistry letters*, 2012, **3**, 3228-3233.
29. Y. Nie, Y. Wang and P. Biswas, *The Journal of Physical Chemistry C*, 2017, **121**, 10529-10537.
30. Z. Tang, X. Li, Z. Han, L. Yao, S. Shen and J. Yang, *RSC Adv.*, 2016, **6**, 87796-87801.
31. E. De Langre, C. N. Baroud and P. Reverdy, *Journal of Fluids and Structures*, 2010, **26**, 205-217.
32. Q. Liu, Y. Gao and B. Xu, *Applied Physics Letters*, 2016, **108**, 141906.
33. Q. Liu and B. Xu, *The Journal of Physical Chemistry C*, 2018.
34. M. Li, Q. Yang, H. Liu, M. Qiu, T. J. Lu and F. Xu, *Small*, 2016, **12**, 4492-4500.
35. Y. Liu and B. I. Yakobson, *Nano letters*, 2010, **10**, 2178-2183.
36. Q. Lu and R. Huang, *Physical Review B*, 2010, **81**.
37. N. Patra, B. Wang and P. Král, *Nano letters*, 2009, **9**, 3766-3771.
38. P. G. de Gennes, *Reviews of Modern Physics*, 1985, **57**, 827-863.
39. S. Alben, B. Balakrisnan and E. Smela, *Nano letters*, 2011, **11**, 2280-2285.
40. T. Werder, J. H. Walther, R. Jaffe, T. Halicioglu and P. Koumoutsakos, *The Journal of Physical Chemistry B*, 2003, **107**, 1345-1352.
41. Y. Zhang, Q. Liu and B. Xu, *Journal of Applied Mechanics*, 2017, **85**, 021006-021006-021009.
42. M. Rivetti and A. Antkowiak, *Soft Matter*, 2013, **9**, 6226.
43. J. Bueno, H. Casquero, Y. Bazilevs and H. Gomez, *Meccanica*, 2017.
44. S. Plimpton, P. Crozier and A. Thompson, *Sandia National Laboratories*, 2007, **18**.
45. P. Mark and L. Nilsson, *The Journal of Physical Chemistry A*, 2001, **105**, 9954-9960.
46. S. J. Stuart, A. B. Tutein and J. A. Harrison, *The Journal of chemical physics*, 2000, **112**, 6472-6486.
47. D. W. Brenner, O. A. Shenderova, J. A. Harrison, S. J. Stuart, B. Ni and S. B. Sinnott, *Journal of Physics: Condensed Matter*, 2002, **14**, 783.
48. T. Werder, J. Walther, R. Jaffe, T. Halicioglu and P. Koumoutsakos, *The Journal of Physical Chemistry B*, 2003, **107**, 1345-1352.

TOC

Liquid evaporation-driven self-folding of 2-D planar free-standing graphene into 2-D or 3-D folded structures is presented in theory and simulations